JGR Earth Surface

RESEARCH ARTICLE
10.1029/2018JF004820

The Effect of Submarine Melting on Calving From Marine Terminating Glaciers

Yue Ma[1] **and Jeremy N. Bassis**[2]

[1]Physics Department, University of Michigan, Ann Arbor, MI, USA, [2]Climate and Space Sciences and Engineering, University of Michigan, Ann Arbor, MI, USA

Key Points:
- We simulate the interplay between submarine melt and calving using a 2-D model of a marine terminating glacier
- Submarine melt can enhance or suppress calving, but the total mass lost (usually) increases
- The magnitude and vertical distribution of submarine melt profile determine if melt enhances or suppresses calving

Correspondence to:
Y. Ma,
yuema@umich.edu

Citation:
Ma, Y., & Bassis, J. N. (2019). The effect of submarine melting on calving from marine terminating glaciers. *Journal of Geophysical Research: Earth Surface*, *124*, 334–346. https://doi.org/10.1029/2018JF004820

Received 21 JUL 2018
Accepted 17 JAN 2019
Accepted article online 21 JAN 2019
Published online 6 FEB 2019

Abstract Submarine melting and iceberg calving are two important processes that control mass loss from the terminus of tidewater glaciers. There have been significant efforts to quantify the effect of submarine melting on glacier calving, but controversy remains with conflicting studies indicating submarine melting can increase, decrease, or has minimal effect on calving. Here we show using a two-dimensional full Stokes finite element model that submarine melt can alter the state of stress near the terminus and the changes in stress exert a first-order control on the calving regime of marine terminating glaciers. The model calculates both the largest principal and maximum shear stresses and then maps out where tensile and shear failure occur for a range of melt rates and vertical melt profiles. We find that submarine melt initially promotes full thickness calving events. However, as the melt rate further increases, an overhang begins to form and resulting compressive stresses suppress full thickness calving. These results are relatively insensitive to basal friction. Moreover, our results suggest that submarine melting can both increase and decrease calving rates with the magnitude and sign of the effect determined by the shape of the melt profile and the relative magnitude of average melt rate. Despite the fact that calving is suppressed in some circumstances, the addition of submarine melt almost always increases the total mass loss. Overall, we find that relatively small amounts of submarine melt can destabilize glaciers, but calving and frontal ablation are increasingly controlled by submarine melt as it continues to increase.

1. Introduction

Iceberg calving and submarine melting are two important processes that occur at the interface between a marine terminating glacier and the ocean. Together, calving and submarine melting—collectively called "frontal ablation"—account for nearly half of the total mass lost from the Greenland Ice Sheet (Enderlin et al., 2014; Rignot et al., 2008; van den Broeke et al., 2009). Despite this important role, our understanding of both processes and, in particular, the interaction between submarine melting and iceberg calving remains limited with different studies finding contradictory relationships (Bartholomaus et al., 2013; Cook et al., 2014; Krug et al., 2015; Luckman et al., 2015; Motyka et al., 2003; O'Leary & Christoffersen, 2013; Rignot et al., 2010, 2016; Röhl, 2006; Todd & Christoffersen, 2014; Truffer & Motyka, 2016). For example, O'Leary and Christoffersen (2013) took a diagnostic approach to examine how frontal melting promotes calving. By developing a two-dimensional finite element model, they concluded that the shift in stress contours resulting from fixed undercutting with various shapes at the terminus is likely to increase calving and is insensitive to the choice of calving law, basal condition (unless floating), or ice thickness. However, their model was limited by its purely diagnostic nature; stress was computed based on rectangular glaciers with specified calving front profiles without accounting for the coevolution of the calving front morphology with melt and ice dynamics. In contrast, several studies allowed calving front morphology to evolve in response to an applied melt rate (Cook et al., 2014; Krug et al., 2015; Todd & Christoffersen, 2014). These studies used more realistic geometries and forcing to examine the role of submarine melting in determining glacier terminus positions. For instance, Cook et al. (2014) modeled Helheim Glacier and found that in their simulations, terminus behavior is not sensitive to the presence of submarine melt unless unrealistically large melt rates were prescribed. Similarly, Todd and Christoffersen (2014) focused on Store Glacier and arrived at a conclusion that submarine melting has a limited effect on calving behavior. In this case, the terminus was perched atop a thick sill and located near a bottleneck in the fjord. Todd and Christoffersen (2014) also reported that despite a slight increase in calving frequency with submarine frontal melting, the simulated size of calving events decreased as submarine melting increased. However, in a more recent study of the same glacier,

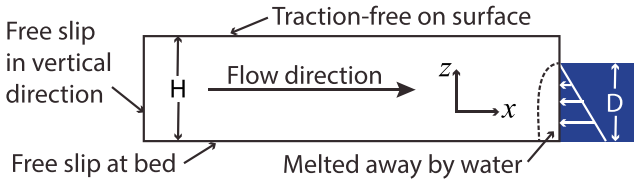

Figure 1. A schematic of the two-dimensional model domain with boundary conditions labeled. The white rectangle represents ice (thickness $H = 800$ m) and the blue rectangle ocean (depth $D = 700$ m). The flow of ice is from left to right in the figure. Our idealized domain consists of (initially) rectangular glaciers on flat beds. Our model neglects basal topography and lateral drag to better isolate the near terminus processes associated with submarine melt.

Todd et al. (2018) concluded using a 3-D model that concentrated plume melting has a destabilizing effect on the calving front position. In contrast, Krug et al. (2015) examined a variety of glacier geometries as well as melt rates and argued that frontal melting did impact terminus behavior on a seasonal time scale, but had no effect on interannual mass loss. They too concluded that undercutting grounded glaciers increased calving frequency but reduced calving size. More recently, Benn et al. (2017) examined the relationship between calving and submarine melting at the calving front using discrete element models that simulate both flow and fracture combined with finite element models of the viscous flow. They found that submarine melt could significantly alter the size of calving events and this effect became dramatically larger as glaciers (or parts of glaciers) became hydrostatically unstable (superbuoyant).

Observational studies have been equally conflicted. For instance, Luckman et al. (2015) discovered a linear dependency of frontal ablation (the combination of submarine melt and calving) on ocean temperature among three Svalbard tidewater glaciers. Bartholomaus et al. (2013) found that the large submarine melt rates during the summer of Yahtse Glacier, Alaska, accounted for nearly all of the mass loss from the terminus region with only a small contribution from calving. This suggests that, at least for these glaciers, submarine melting is the dominant process controlling frontal ablation. However, observations also show that frontal ablation strongly correlates with near terminus velocity (van der Veen, 2002). In this case, it is unclear why submarine melt, largely controlled by ocean properties, would correlate with terminus velocity, which is determined by ice dynamics. Furthermore, melt rates in many cases are much smaller than daily ice flow velocities, which can be up to tens of meters per day at many rapidly flowing outlet and tidewater glaciers (Moon et al., 2014, 2012; Rignot & Kanagaratnam, 2006). For example, terminus velocities for Jakobshavn Isbræ approach 34 m/day (Joughin et al., 2004, 2008), while submarine melt rates are no greater than 3 m/day (Enderlin & Howat, 2013). This has led researchers to suggest that submarine melt is less important—or negligible—for these large outlet glaciers.

Here we seek to address this controversy using an idealized glacier model to simulate the interaction between submarine melting, ice dynamics, and calving. Our model, a two-dimensional Stokes flow based on the finite element analysis (described in more detail below), was developed to examine both tensile and shear failure regimes within glaciers and tracks the growth of surface and basal crevasses (Ma et al., 2017). In this study we apply a similar methodology but additionally prescribe submarine melting to examine how erosion of the calving front alters the shape of the glacier and through it, the stress regime.

2. Model Description

For computational simplicity and to illuminate relevant processes, we focus on a two-dimensional flow model that consists of a vertical cross section, which cuts along the central flow line of a glacier (Figure 1). We use this two-dimensional model to characterize calving behavior, focusing on the near terminus region where icebergs detach.

2.1. Ice Dynamics

As described in Ma et al. (2017), the full Stokes system we are solving can be represented as the conservation of linear momentum in both x and z directions and the incompressibility of glacier ice:

$$\frac{\partial \tau_{xx}}{\partial x} + \frac{\partial \tau_{xz}}{\partial z} = \frac{\partial p}{\partial x}, \tag{1}$$

$$\frac{\partial \tau_{xz}}{\partial x} + \frac{\partial \tau_{zz}}{\partial z} = \frac{\partial p}{\partial z} + \rho_i g, \tag{2}$$

$$\frac{\partial u}{\partial x} + \frac{\partial w}{\partial z} = 0. \tag{3}$$

Here we denote the components of the deviatoric stress tensor by τ_{ij} where $(i, j) = (x, z)$, pressure by p, density of ice by ρ_i (see Table 1), and gravitational acceleration by g, with x representing the along-flow coordinate and z representing the vertical coordinate, as illustrated in Figure 1.

Table 1
Physical Parameters Used in Experiments

Parameter	Value
Initial ice thickness H	800 m
Initial length to thickness ratio L/H	6
Water depth D	700 m
Gravitational acceleration g	9.8 m/s^2
Depth-averaged melt rate $\bar{m}$	0.05–5.0 m/day
Glacier temperature T	−20 °C
Temperature-dependent creep parameter B	4.088×10^6 Pa·day$^{1/3}$
Density of ice ρ_i	910 kg/m^3
Density of sea water ρ_w	1,020 kg/m^3
Friction coefficient μ	2.0×10^5 Pa·m^{-1}·day

The connection between strain rate and deviatoric stress is given by the rheology of ice, in the form of a power law (Glen, 1955; Nye, 1955),

$$\tau_{ij} = B\dot{\epsilon}_e^{\frac{1-n}{n}}\dot{\epsilon}_{ij} \tag{4}$$

where $\dot{\epsilon}_{ij}$ denotes the strain rate components and $\dot{\epsilon}_e$ denotes the second strain rate invariant, defined by $2\dot{\epsilon}_e^2 = \dot{\epsilon}_{ij}\dot{\epsilon}_{ij}$. Here B is the temperature-dependent creep parameter defined in van der Veen (2013, Chapter 2; see Table 1), and $n = 3$ denotes the creep exponent. There are four boundary conditions that need to be defined: surface, bed, upstream, and downstream/terminus. Because atmospheric pressure is (nearly) constant over the glacier, the ice-air interface is treated as traction free. Moreover, since we only consider short time intervals such as months to a year, we do not include surface mass balance in our simulations. At the ice-water interface (terminus), we insist on continuity of traction, assuming that ocean water is in hydrostatic equilibrium. Because our primary interest is in grounded tidewater glaciers, we focus only on the evolution of glaciers up to flotation. Once the ice thickness reaches buoyancy, the model is stopped. At the bed, we apply a Newtonian sliding law with a constant friction coefficient μ:

$$f = \mu u. \tag{5}$$

We considers two cases. The first case corresponds to negligible resistance from sliding ($\mu = 0$), while the second case incorporates sliding appropriate for a fast flowing outlet glaciers (see Table 1).

For the upstream (inflow) boundary condition, we assume free-slip in the vertical direction and zero horizontal inflow velocity. Both tensile and shear stress fields are calculated diagnostically and examined to determine where failure occurs. The failure criteria we apply are described below in section 2.2, and the model numerics are described in more details in section 2.4.

2.2. Failure Criteria

In the section above we have focused on the deviatoric stress. However, the failure criteria are based on the Cauchy stress and we examine both tensile and shear stresses (Ma et al., 2017). The relationship between Cauchy stress σ and deviatoric stress τ is simple:

$$\sigma_{ij} = \tau_{ij} - p\delta_{ij} \tag{6}$$

where p is the pressure and δ_{ij} is the Kronecker delta. The eigenvalues of the Cauchy stress tensor give the two principal stresses

$$\sigma_{\max,\min} = \frac{\sigma_{xx} + \sigma_{zz}}{2} \pm \sqrt{\left(\frac{\sigma_{xx} - \sigma_{zz}}{2}\right)^2 + \sigma_{xz}^2} \tag{7}$$

The difference between the two principal stresses gives the maximum shear stress

$$\tau_{\max} = \frac{1}{2}\left(\sigma_{\max} - \sigma_{\min}\right) = \sqrt{\left(\frac{\sigma_{xx} - \sigma_{zz}}{2}\right)^2 + \sigma_{xz}^2} \tag{8}$$

Because crevasses are largely tensile fractures, high tensile stress naturally promotes their growth. Following previous work (e.g., Benn et al., 2007; Nick et al., 2010; Nye, 1955), crevasses grow when the largest principal stress σ_{max} is positive and penetrates to the depth where the largest principal stress becomes compressive. This model, frequently termed the "Nye zero stress" model, corresponds to the assumption that (i) crevasses are closely spaced so that they do not significantly alter the large-scale stress field and (ii) preexisting flaws are prevalent allowing crevasses to initiate anywhere and penetrate to the deepest portion of the glacier permissible based on the stress regime. We include both surface and basal crevasses in our treatment. Surface crevasses in our model are assumed to be water free. The presence of water in surface crevasses would enable them to penetrate more deeply, but few measurements exist that constrain water depth in crevasses. Moreover, iceberg calving events do occur in regions and time periods where atmospheric temperatures are too cold to support water filled crevasses. Basal crevasses near the terminus are assumed to be connected to the ocean and thus filled by seawater. Hence, water pressure from the ocean is added to the existing stress field for the area of the glacier below the waterline, analogous to the treatment by Benn et al. (2017). Therefore, zones where the largest principal stress is positive ($\sigma_{max} > 0$) suggest areas where crevasses can exist, with the zero stress contour marking the boundary between crevassed and uncrevassed ice.

High shear stress also promotes failure along faults. Ice has been postulated to fail when the maximum shear stress τ_{max} exceeds the shear strength, which field and laboratory studies suggest falls in the range of 500 kPa to 1 MPa (Bassis & Walker, 2012; Frederking et al., 1988; Morlighem et al., 2016; Petrovic, 2003; Schulson, 1999). We use a value of 500 kPa in our model. Similar to how we treat tensile stress, again assuming dense preexisting flaws and narrow faults, the maximum shear stress is calculated and areas of high shear stress, that is, with values above the shear strength of ice ($\tau_{max} > 500$ kPa), are identified.

In addition to the above two-stress criterion, we assume that the history of the ice can affect its current state. Studies have shown that crevasses generally remain open during glacier advection for about 1–2 years (Colgan et al., 2016; Harper et al., 1998), which is longer than or at least equivalent to the time scale we consider in this study (several months to a year). Therefore, once ice becomes crevassed in the model, we assume it stays crevassed. The area of crevassed (failed) ice at any time step is the sum of that from all the previous time steps, reflecting the history of the glacier stress field.

2.3. Imposed Submarine Melt

High-resolution three-dimensional ocean circulation models can describe submarine melting, but the demand for high computational power as well as the uncertainty in appropriate far field forcing and local subglacial discharge associated with these simulations makes simplified profiles more suitable for our purpose. Here we approximate submarine melting using three idealized melt profiles and compare glacier response to different profile shapes and average melt rates.

Some studies have shown melt rates reaching a maximum near the lower part of the calving front caused by the penetration of warm, dense intermediate waters that are quickly cooled by the entrainment of cold, fresh water generated by ice melt (e.g., Rignot et al., 2015; Sciascia et al., 2013; Xu et al., 2013). To approximate this type of profile, we assume the submarine melt rate increases linearly from 0 at the waterline to a maximum value at the bed:

$$\dot{m} = 2\bar{\dot{m}}(1 - \frac{z}{D}) \tag{9}$$

where $\bar{\dot{m}}$ is the depth-averaged value of the melt rate, D is the water depth, and z is the vertical position with $z = 0$ at the bed and $z = D$ at the waterline.

In contrast, a melt rate maximum near the middle part of the calving front is also possible (e.g., Rignot et al., 2015; Sciascia et al., 2013; Slater et al., 2017), with shapes of melt profiles resembling a parabola. In this case, the melt rate is zero both at the waterline and the bed and reaches a maximum between the bed and ocean surface. We approximate this melt profile as follows:

$$\dot{m} = 6\bar{\dot{m}}\frac{z}{D}(1 - \frac{z}{D}). \tag{10}$$

Finally, the third choice is simply a uniform melt profile where the melt rate stays constant from the waterline to the bed:

$$\dot{m} = \bar{\dot{m}}. \tag{11}$$

Constant melt may be representative of shallow termini or really warm waters found in some Alaskan fjords.

These melt profiles are all idealized and unlikely to exactly resemble the melt rate at any particular glacier, but a combination of all three can approximate many scenarios of submarine melting. However, because our goal is to examine how changes in the shape of the profile and average melt rate $\bar{m}$ alter the stress field within the glacier, simple melt profiles serve the purpose better than more detailed submarine melt parameterizations.

Typical submarine melt rates around Greenland are seasonal but have values ranging from 0.1 to 10 m/day (Truffer & Motyka, 2016). We examine rates between 0.05 and 5 m/day. Submarine melt is applied normal to the calving front.

2.4. Model Numerics and Initial Conditions

We use the open source FEniCS package (Alnæs et al., 2015; Logg et al., 2012) to solve the stress equilibrium equations combined with appropriate boundary conditions and the rheology of ice (section 2.1). Each glacier was initialized as an isothermal rectangular slab on a flat bed with prescribed thickness and water depth. The initial thickness of the glacier is set to 800 m, as a representative size of major marine terminating glaciers in Greenland and Alaska (e.g., Jakobshavn, Helheim Glacier). Based on our failure criterion, only a range of ice thickness/water depth combinations are permissible at the calving front or the glacier will develop through-penetrating fractures immediately, resulting in disintegration (Ma et al., 2017). This envelope of ice thickness/water depth combinations also agrees with observations around Greenland (Bassis & Walker, 2012; Ma et al., 2017). The range of water depth allowed by the stable envelope is about 90% of the ice thickness (buoyancy level) to 10–100 m below it. Here, the choice of water depths (700 m) is a bit below the buoyancy level (714 m) and the modeled glacier falls well within the stable envelope. Because our interest lies in the near terminus region, we set the initial length in each simulation to 6 times the thickness to avoid edge effects associated with the upstream boundary condition; we experimented with different aspect ratios and found that the stress field near the calving front was insensitive to the length above this threshold. We use a mesh of triangular elements and a resolution of 2% of the initial glacier thickness uniformly in both vertical and horizontal directions. At this resolution our results are insensitive to a factor of 2 changes in resolution. During each time step (a quarter of a day), the tensile and shear stress fields are calculated from the velocity solution to determine areas within the glacier that satisfy the tensile or shear failure criteria (section 2.2). Then we advect all nodes using the nodal velocity vector and erode the portion of the calving front submerged in water according to the imposed submarine melt profile. At the end of each time step, we remesh according to the updated glacier outline to maintain a constant mesh quality throughout the simulation. The program is stopped once a calving event has been observed.

3. Results

3.1. Effect of Melt Profile Shape on Stress Regime

We first examined how changes in the shape of the glacier affect the stress field as the glacier and calving front coevolve as a function of different melt rates and profiles. Figure 2 shows three snapshots from examples: with no submarine melt, a parabolic melt profile (mean melt rate 0.5 m/day), and a uniform melt profile (melt rate 0.5 m/day) for an initially 800-m-thick glacier grounded in 700 m of water. Initially, failure (mostly tensile) is concentrated in portions of the glacier above the waterline as well as near the bed and extends deeper into the glacier closer to the terminus (Figure 2, left column). This is a consequence of our assumption that ocean water fills all basal crevasses. For the case where no melting is applied, the failure zone near the bed slowly expands and connects to the surface as the glacier thins to near buoyancy (Figure 2, top middle and top right panels). When submarine melting is introduced, stress patterns become more complex and depend more sensitively on the shape of the profile.

The pattern of stress also depends on the amplitude of submarine melt. This is illustrated in Figure 3, which shows the stress regime at the point of calving for two different mean submarine melt rates. For the linear profile (row A in Figure 3), increased submarine melt results in higher tensile stresses (later high shear stress too) and leads to larger regions of failure that connect between the surface and bottom of the glacier. In this case, submarine melt acts to increase stress and hence to promote calving. In contrast, for the parabolic and uniform profiles (middle row in Figure 2 and rows B and C in Figure 3), a pronounced overhang develops and the flexure associated with the overhang creates compressive stress near the bottom of the glacier, reducing the area where full thickness failure can occur and the stress regime near the calving front right beneath the

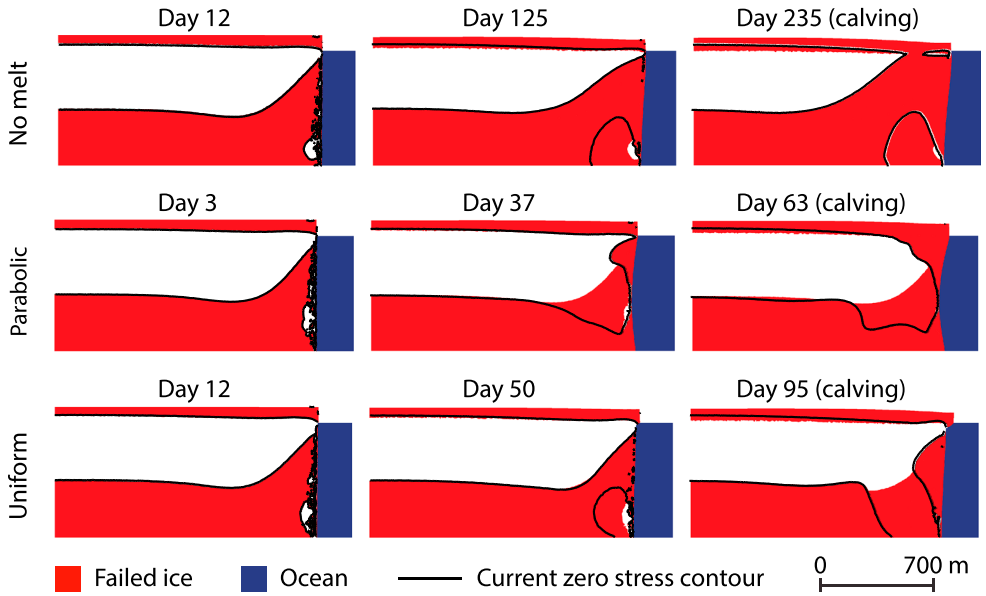

Figure 2. The evolution of stress within a tidewater glacier without basal friction. The initially 800-m-thick glacier is flowing from left to right, into 700-m-deep ocean (indicated by blue). These panels are cropped to show only the section of the glacier close to the calving front. Solid black lines indicate the Nye zero stress contour at the current time. The red shaded area shows accumulation of ice that has failed, reflecting the evolution and history of the glacier. White regions indicate zones of intact ice. When zones of failed ice connect, a calving event occurs. Top row shows three snap shots throughout the course to calving when there is no submarine melting. The middle and bottom rows show the case of a parabolic and uniform melt profile, respectively, with an average melt rate of 0.5 m/day. The first column shows the stress field at the beginning of the simulation. The second column shows the stress distribution at a point intermediate to a calving. The third column shows a situation where failed ice penetrates the entire ice thickness and a calving event occurs.

developing overhang has become compressive. Compared to the linear profile, full thickness calving events simulated for the parabolic and uniform profiles are smaller in size (Figure 3, panels IB and IIB). However, as the overhang becomes more pronounced, stresses (especially shear stress) within the overhang increase and can lead to another type of calving events: overhang collapse. This is especially true for the uniform melt profile when the melt rate is relatively high (Figure 3, IIC). The same compressive stress regime can be seen from the zero stress contours (Figure 2, bottom row last panel). In summary, we see two modes of calving: full thickness calving and overhang collapse. The type of calving event is determined by both the magnitude and shape of the melt profile.

3.2. Effect of Submarine Melting on Calving and Frontal Ablation

We next sought to quantify the effect of submarine melting on the rate at which ice is lost due to calving along with the total mass lost due to frontal ablation. To do this, we crudely define the "calving rate" c as the area Q_c of ice breaking off divided by the time t it takes in our simulation for the ice to reach a state where failure can result in the detachment of an iceberg:

$$c = \frac{Q_c}{t} \tag{12}$$

This leads to the definition of "frontal ablation rate" or "total mass loss rate" a to be the sum of calving rate and the product of melt rate $\dot{m}$ and water depth D:

$$a = c + \dot{m}D \tag{13}$$

We use the term calving rate and frontal ablation rate loosely to quantify the temporal change in the stress regime associated with the emergence of through-penetrating fractures with and without submarine melting. Long-term calving rates depend on upstream boundary condition and climate forcing, processes that are not accounted for in our idealized model.

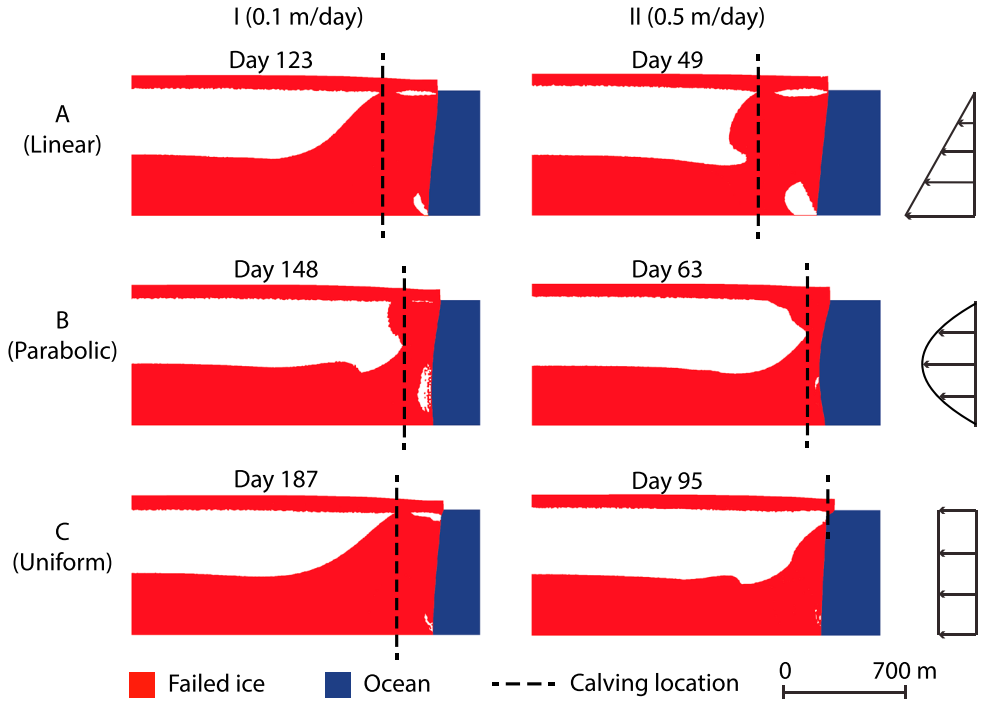

Figure 3. Snapshots of zones of failed ice within a tidewater glacier at times of calving events absent of basal friction. The initially 800-m-thick glacier is flowing from left to right, into 700-m-deep ocean (indicated by blue). These panels are cropped to show only the section of the glacier close to the calving front. Red indicates failed ice, and white is intact ice. Dashed black lines indicate locations of iceberg detachment when failed ice penetrates the entire ice thickness. Rows A–C show calving events under a linear, parabolic, and uniform melt profile, respectively (sketched in the rightmost panels). Columns I and II each corresponds to a different depth-averaged melt rate: 0.1 and 0.5 m/day, respectively. Panels IA, IIA, and IC show examples of a full thickness calving event. Panels IB and IIB show examples of a smaller full thickness calving event. Panel IIC shows an example of an overhang break-off.

Because our interest is in the role that submarine melt plays in enhancing or reducing the time it takes to develop through-penetrating fractures, we define a "calving rate multiplier" β_c as the ratio of calving rate with submarine melting c_m to that without submarine melting c_0:

$$\beta_c = \frac{c_m}{c_0}. \tag{14}$$

Similarly, we define a frontal ablation multiplier β_f as the ratio of total mass loss rate with submarine melting a_m to that without submarine melting a_0:

$$\beta_f = \frac{a_m}{a_0} = \frac{c_m + \dot{m}D}{c_0} = \beta_c + \frac{\dot{m}D}{c_0}. \tag{15}$$

Here, a calving rate multiplier or frontal ablation multiplier greater than 1 ($\beta_c > 1$ or $\beta_f > 1$) indicates enhanced calving or frontal ablation relative to the submarine melt free case. In contrast, values less than 1 indicate suppressed calving or frontal ablation relative to the submarine melt free case.

Figure 4 shows the calving rate and frontal ablation rate multiplier as a function of submarine melt rates ranging from 0 (no melting) to 2 m/day when there is no basal friction. The data points for the 5-m/day melt rate are not included in the figure, but the trend holds. We see three distinct responses in the simulations when the three melt profiles are applied. Applying a linear melt profile results in an almost linear increase in both calving and frontal ablation enhancement with increasing melt rates. In contrast, applying a uniform melt profile results in an initially nearly linear increase for low melt rates followed by a sharp dropoff above a threshold melt rate and then a linear increase again as melt rates further increase. Finally, applying a parabolic melt profile results in a slight decrease for low melt rates followed by a linear increase above a threshold melt rate. The specific value of the multiplier, however, depends on the shape of profile with the

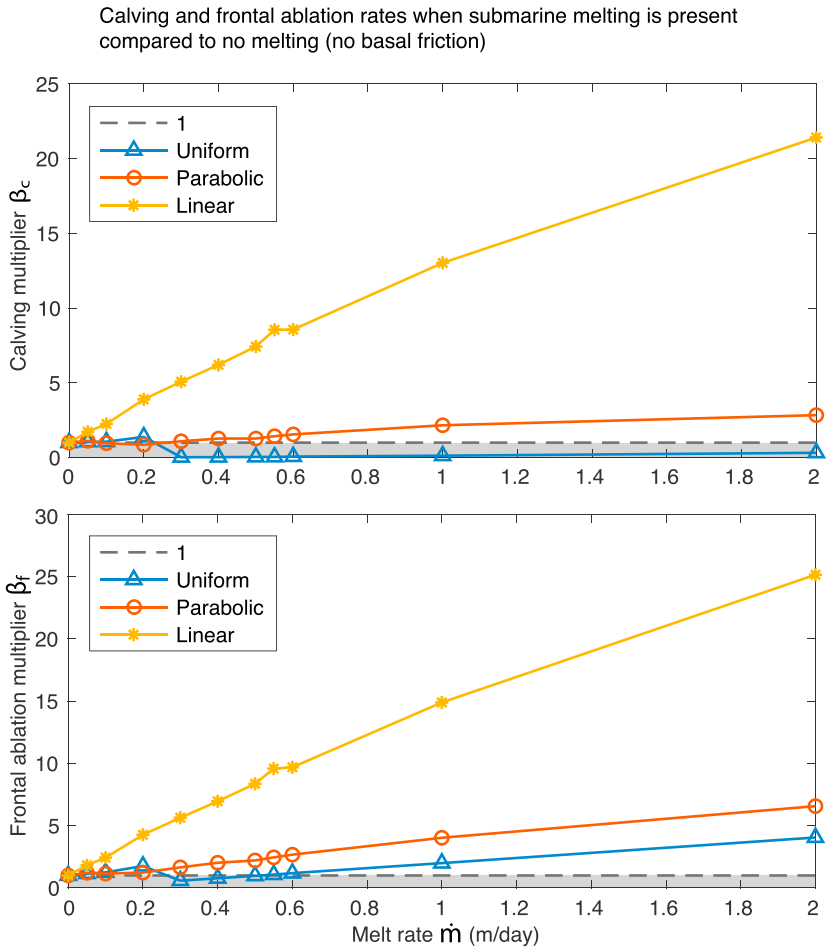

Figure 4. The effect of submarine melt on calving and frontal ablation when there is no basal friction. The top panel shows the influence of submarine melt on the calving rate multiplier, while the bottom panel shows the frontal ablation rate multiplier. Yellow (stars), red (circles), and blue (triangles) lines correspond to linear, parabolic, and uniform melt profiles. The dashed line in both panels indicates a value of 1. It separates enhancement (values above the line) from suppression (values beneath the line in the shaded area).

linear melt profile resulting in as much as a twentyfold increase in calving rate and frontal ablation rate. This should be contrasted with the uniform and parabolic profiles, which result in more modest maximum enhancements of $\sim$ 200% and 10%, respectively. For the parabolic profile, below $\sim$ 0.3 m/day, the smaller berg sizes result in a small drop in calving rate multiplier. In this regime, submarine melting suppresses mass lost due to calving. We see an opposite trend for the uniform melt rate at the same melt rate. In this case, a prominent overhang develops. Bending associated with the unsupported overhang increases the compressive stress in the portion of the glacier below the overhang, and high tensile and shear stress are concentrated in the overhang, resulting in the overhang break-off from the main body of ice instead of a full thickness calving event. The uniform and parabolic melt profiles suppress calving for certain melt rates, but with added mass loss through submarine melting we see a frontal ablation rate comparable to or higher than that without submarine melting (ratio about equal to or greater than 1), except for a narrow range of melt rates for the uniform melt profile.

3.3. Effect of Basal Friction

Our free-slip experiments represent significant idealizations. To examine the effect of basal friction on our results, we also performed a set of simulations with a Newtonian sliding law. We set the coefficient of friction such that the magnitude of basal friction is between 50 and 100 kPa. The stress field when a calving event occurs in this case is very similar to that without basal friction for almost all cases, except for the parabolic melt profile. The difference in the stress field at the time of calving between the friction case and

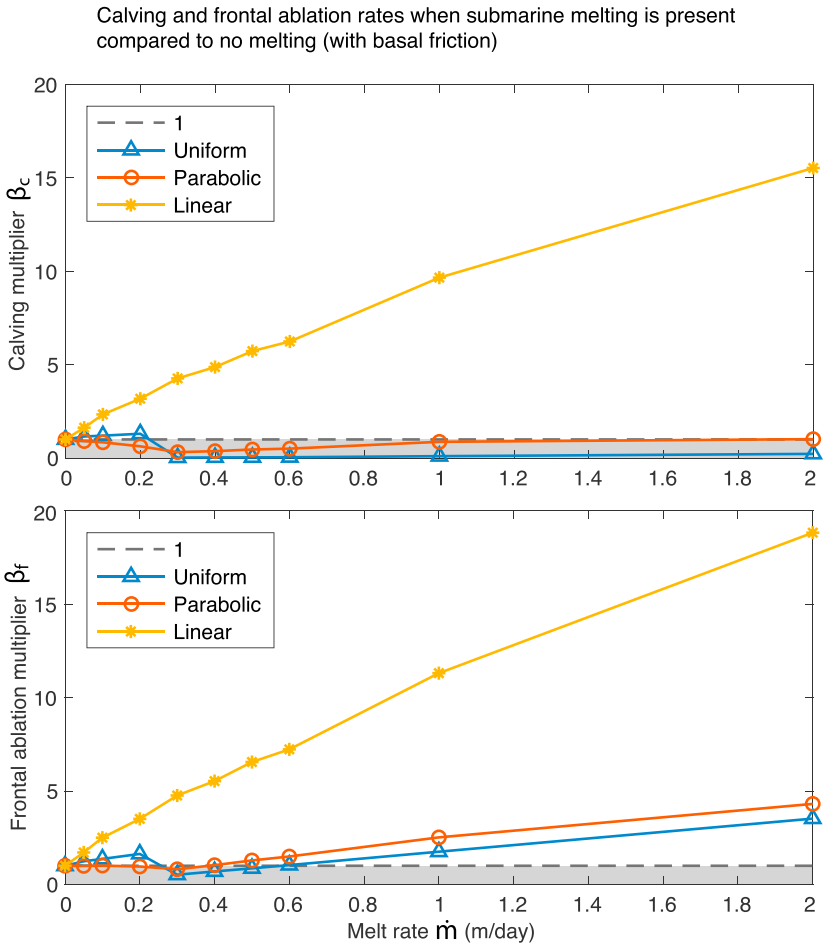

Figure 5. The effect of submarine melt on calving and frontal ablation when there is basal friction. The top panel shows the influence of submarine melt on the calving rate multiplier, while the bottom panel shows the frontal ablation rate multiplier. Yellow (stars), red (circles), and blue (triangles) lines correspond to linear, parabolic, and uniform melt profiles. The dashed line in both panels indicates a value of 1 separating enhancement (values above the line) from suppression (values beneath the line in the shaded area).

the friction-free case is that the former shows larger compressive stress at the bottom of the glacier near the calving front, while the latter shows tensile stress. The inclusion of friction decreases the velocity of ice at the ice-bed interface, and this results in larger compressive stresses. Consequently, comparing Figure 5 with Figure 4, we see that the calving behavior corresponding to each melt profile remains qualitatively similar regardless of basal friction and the monotonic increase for the linear melt profile, the slow increase after decrease for the parabolic melt profile, as well as the decrease after the initial increase for the uniform profile are still present. However, the magnitude of the calving and frontal ablation multipliers are slightly smaller and the transition melt rate between enhancement and suppression of calving for the parabolic and uniform melt profiles shifts to $\sim$ 0.2 m/day. Moreover, the calving multiplier for the parabolic profile when basal friction is present is lower compared to the case with no friction for melt rates up to 2 m/day. The resistance at the bed creates a more compressive stress regime near the bottom part of the glacier, making it more difficult for failure zones to extend and connect throughout the entire ice thickness. We anticipate that more complex basal sliding laws would affect our quantitative results but that we would see similar qualitative trends so long as the glacier remains in the rapidly sliding regime.

3.4. Multiple Calving Events

Our idealized simulations all started with rectangular geometries, and thus, the first calving event in our model may not be representative of the true calving rate. To examine the effect of multiple calving events, we performed a final simulation in which we simulated a second calving event after the initial break-off event. To do this, we simulated calving events by instantaneously removing all ice seaward of the location where

we simulate through-penetrating fractures. In the absence of submarine melt, our simulated glacier evolves until it reaches buoyancy without experiencing another calving event. In contrast, when submarine melt is applied to the calving front, the shape of the calving front continues to evolve and we do observe a second calving event before the glacier reaches buoyancy. For modest melt rates between 0.1 and 0.5 m/day this second calving event takes longer than the first calving event, but faster than in the absence of submarine melt (where we do not observe a second calving event prior to the formation of a floating ice tongue). In these cases, submarine melt appears to enhance total front ablation. However, these simulations do not account for buoyancy induced calving, which could result in through penetration fractures upstream of the calving front when the glacier approaches flotation. This suggests that, qualitatively at least, submarine melt may enhance total frontal ablation for multiple calving events. However, our estimated long-term calving fluxes are less certain because the longer time scale evolution of the glacier associated with multiple calving events depends on a group of factors that we have not considered. For example, the effect of surface mass balance and variations in bed geometry are likely to become more important in controlling the timing of calving events when the modeled time period extends well beyond 1 year. Instead, our simulations show that submarine melt alters the geometry of the calving front and this change in geometry has a first-order effect on the stress regime near the calving front and this change is likely to translate into a change in the calving rate of glaciers.

4. Discussion

Our simulations show that submarine melting, by changing the morphology of the calving front, exerts a first-order control on the near terminus stress regime state of marine terminating glaciers. This effect can, in some cases, increase or suppress calving. The magnitude—and even the sign of the interaction between submarine melting and calving—depends on both the amount of submarine melt and the vertical distribution of melt over the calving front. The shape of the melt profile plays such an important role in determining the interplay between calving and submarine melting because of the effects different melt profiles have on the shape of the calving face. Undercutting at the calving front results in unsupported mass; the size and shape of this mass can result in stabilizing compressive stresses upstream from the overhang or destabilizing tensile stresses close to the calving front. The uniform melt profile case is most effective in suppressing calving; the linear melt profile tends to enhance calving. Ultimately, however, the overhang grows large enough that it becomes unstable and detaches.

Our simulations identify different types of calving in response to submarine melting. When submarine melting is present, the erosion of ice from the calving front allows glacier ice to flow into the calving front and partially compensate for the change in the shape of the calving front. Consequently, the glacier thins faster and reaches a full thickness calving event earlier in our simulations than in the absence of submarine melt. Because more glacier ice is being removed from the calving front halfway underwater than at the waterline or the bottom, the parabolic melt profile renders the extra mass near the surface unsupported so that the stress field becomes more compressive, resulting in a slightly reduced calving event size. As the melt rate further increases, the time to calving reduces. Although the calving size shows little change, calving rate increases with melt rate. For the uniform melt profile case, when enough mass is removed from the calving front below the waterline, a large overhang develops. Similar to the parabolic case, the unsupported overhang has a compressive effect on the part of ice underneath it and is less favorable for the growth of tensile failure. Nonetheless, the portion where the overhang connects to the main body of ice becomes more prone to failure due to a concentrated area of high shear and high tensile stress around the entire overhang. The more rapidly ice is melted away, the earlier the overhang becomes large enough to detach. The linear submarine melt profile case is different from the other two cases because removing more ice from the bottom and creating a sloping calving front promotes full thickness calving by increasing the calving size significantly. The faster ice is being removed from the bottom, the more unstable the calving front becomes and the easier it is for a full thickness calving event to occur.

Our results are relatively consistent with observations. For example, Bartholomaus et al. (2013) found that, at least during the summer when ocean temperatures were large (> 10 °C), the mass lost from Yahtse Glacier, Alaska, due to submarine melting accounted for nearly all of the submarine mass loss. This corresponds to our simulations where submarine melt rates are large compared to the ice flow velocity—especially if submarine melt rates are approximately uniform along the calving front. Our model would predict this regime is controlled by overhang collapse, although narrow full thickness bergs could also occasionally

detach. Similarly, our model is consistent with the relatively warm ocean temperatures controlling frontal ablation of Svalbard glaciers (Luckman et al., 2015) because frontal ablation is controlled by submarine melting for large melt rates.

The most intriguing result from our simulations is that submarine melt can both increase and reduce calving, depending on the shape of the melt profile. An initial increase in melt rate can increase calving for the uniform profile. However, as the melt rate continues to increase, we see a transition to smaller icebergs and this reduced iceberg size decreases the mass lost due to calving. On the other hand, slightly reduced calving has been shown from the model results for small melt rates using the parabolic melt profile because of the slightly reduced size of icebergs. Eventually, as the submarine melt continues to increase, calving flux increases again; this is a consequence of the fact that smaller bergs detach more frequently. Both the uniform and parabolic melt profiles can moderately increase calving. In contrast, for the linear profile, we see increased calving for all melt rates and more than an order of magnitude increase for higher melt rates. This may partly explain the increased calving many tidewater glaciers experience during the summer (e.g., Amundson et al., 2010, 2008), although our model neglects water in surface crevasses and the presence of mélange that has been speculated to buttress the calving front. Despite the fact that submarine melting can suppress calving, the rate of total frontal ablation generally increases with increasing melt rate—with the exception of a narrow range of melt rates. Submarine melt, however, does alter the total frontal ablation along with the partitioning between calving and melting.

5. Conclusion

Our simulations show that vertical distribution of submarine melt along the calving front results in markedly different glaciological stress regimes. A consequence of this is that submarine melting can increase calving by more than an order of magnitude or suppress calving (nearly) entirely, according to our estimate of calving rate based on the first calving event. The distinction between these two effects is controlled by the relative strength of depth-averaged melt rate and, more significantly, the vertical distribution of submarine melt. Although we imposed idealized melt profiles in our simulations, future simulations could more accurately model the interplay between calving and submarine melting either using full ocean circulation models or simpler plume models coupled with an ice sheet model.

Our results also suggest that attempts to understand the interplay between calving and submarine melting need to consider factors that affect the local melt profile and its magnitude along with the effect these have on the glaciological stress regime response. Because of the dependence on the magnitude and vertical distribution of the submarine melt profile, extrapolating observational results from a single or small set of glaciers could prove to be misleading. Moreover, as Luckman et al. (2015) and Rignot et al. (2016) both pointed out, the importance of submarine frontal melting depends on its relative strength compared to ice dynamics at the glacier terminus. Removing ice from the calving front can destabilize the glacier and cause ice to flow into the terminus area to compensate for the effect of melting. However, if the mass is being eroded away too quickly, the resulting instability could be hard to compensate for and a transition from full thickness bergs to smaller bergs or overhang collapse could occur.

Our model is relatively simple and omits several important processes, including lateral geometry and mass balance. Nonetheless, when considering the evolution of glaciers in a warming climate, we may need to consider more than just the magnitude of submarine melt; we may also need to know the precise three-dimensional shape. This, in turn, will require a more in-depth knowledge of the three-dimensional circulation of water in fjords and perhaps more detailed coupling between ice sheet/glacier models and ocean models.

Acknowledgments
We would like to thank the Editors and both reviewers. This work was supported by National Science Foundation grant ANT 114085, National Oceanic and Atmospheric Administration, Climate Process Team: Iceberg Calving grant NA13OAR4310096, and National Science Foundation grant PLR-131568. All numerical information is provided in the tables and figures and was produced by solving the equations stated in the paper. Codes used to generate the results can be found on GitHub at https://goo.gl/R4DwVZ.

References

Alnæs, M. S., Blechta, J., Hake, J., Johansson, A., Kehlet, B., Logg, A., et al. (2015). The FEniCS project version 1.5. *Archive of Numerical Software*, *3*(100), 9–23. https://doi.org/10.11588/ans.2015.100.20553

Amundson, J. M., Fahnestock, M., Truffer, M., Brown, J., Lüthi, M. P., & Motyka, R. J. (2010). Ice mélange dynamics and implications for terminus stability, Jakobshavn Isbræ, Greenland. *Journal of Geophysical Research*, *115*, F01005. https://doi.org/10.1029/2009JF001405

Amundson, J., Truffer, M., Lüthi, M., Fahnestock, M., West, M., & Motyka, R. (2008). Glacier, fjord, and seismic response to recent large calving events, Jakobshavn Isbræ, Greenland. *Geophysical Research Letters*, *35*, L22501. https://doi.org/10.1029/2008GL035281

Bartholomaus, T. C., Larsen, C. F., & O'Neel, S. (2013). Does calving matter? Evidence for significant submarine melt. *Earth and Planetary Science Letters*, *380*, 21–30.

Bassis, J. N., & Walker, C. C. (2012). Upper and lower limits on the stability of calving glaciers from the yield strength envelope of ice. *Proceedings of the Royal Society of London A: Mathematical, Physical and Engineering Sciences*, *468*(2140), 913–931.

Benn, D. I., Åström, J., Zwinger, T., Todd, J., Nick, F. M., Cook, S., et al. (2017). Melt-under-cutting and buoyancy-driven calving from tidewater glaciers: New insights from discrete element and continuum model simulations. *Journal of Glaciology*, *63*(240), 691–702.

Benn, D. I., Warren, C. R., & Mottram, R. H. (2007). Calving processes and the dynamics of calving glaciers. *Earth-Science Reviews*, *82*(3), 143–179.

Colgan, W., Rajaram, H., Abdalati, W., McCutchan, C., Mottram, R., Moussavi, M. S., & Grigsby, S. (2016). Glacier crevasses: Observations, models, and mass balance implications. *Reviews of Geophysics*, *54*, 119–161. https://doi.org/10.1002/2015RG000504

Cook, S., Rutt, I., Murray, T., Luckman, A., Zwinger, T., Selmes, N., et al. (2014). Modelling environmental influences on calving at Helheim glacier in eastern Greenland. *The Cryosphere*, *8*(3), 827–841.

Enderlin, E. M., & Howat, I. M. (2013). Submarine melt rate estimates for floating termini of Greenland outlet glaciers (2000–2010). *Journal of Glaciology*, *59*(213), 67–75.

Enderlin, E. M., Howat, I. M., Jeong, S., Noh, M.-J., Angelen, J. H., & Broeke, M. R. (2014). An improved mass budget for the Greenland Ice Sheet. *Geophysical Research Letters*, *41*, 866–872. https://doi.org/10.1002/2013GL059010

Frederking, R. M. W., Svec, O. J., & Timco, G. W. (1988). On measuring the shear strength of ice. Sapporo, Japan: National Research Council Canada, Institute for Research in Construction. Retrieved from https://nrc-publications.canada.ca/eng/view/accepted/?id=11f59b37-ce0c-425e-a802-97e1a170daa2

Glen, J. W. (1955). The creep of polycrystalline ice. *Proceedings of the Royal Society of London A: Mathematical, Physical and Engineering Sciences*, *228*(1175), 519–538.

Harper, J. T., Humphrey, N., & Pfeffer, W. T. (1998). Crevasse patterns and the strain-rate tensor: A high-resolution comparison. *Journal of Glaciology*, *44*(146), 68–76.

Joughin, I., Abdalati, W., & Fahnestock, M. (2004). Large fluctuations in speed on Greenland's Jakobshavn Isbræ glacier. *Nature*, *432*(7017), 608–610.

Joughin, I., Howat, I. M., Fahnestock, M., Smith, B., Krabill, W., Alley, R. B., et al. (2008). Continued evolution of Jakobshavn Isbræ following its rapid speedup. *Journal of Geophysical Research*, *113*, F04006. https://doi.org/10.1029/2008JF001023

Krug, J., Durand, G., Gagliardini, O., & Weiss, J. (2015). Modelling the impact of submarine frontal melting and ice mélange on glacier dynamics. *The Cryosphere*, *9*, 989–1003.

Logg, A., Mardal, K.-A., & Wells, G. N. (2012). *Automated solution of differential equations by the finite element method*. Berlin: Springer. https://doi.org/10.1007/978-3-642-23099-8

Luckman, A., Benn, D. I., Cottier, F., Bevan, S., Nilsen, F., & Inall, M. (2015). Calving rates at tidewater glaciers vary strongly with ocean temperature. *Nature Communications*, *6*, 8566–8572.

Ma, Y., Tripathy, C. S., & Bassis, J. N. (2017). Bounds on the calving cliff height of marine terminating glaciers. *Geophysical Research Letters*, *44*, 1369–1375. https://doi.org/10.1002/2016GL071560

Moon, T., Joughin, I., Smith, B., Broeke, M. R., Berg, W. J., Noël, B., & Usher, M. (2014). Distinct patterns of seasonal Greenland glacier velocity. *Geophysical research letters*, *41*, 7209–7216. https://doi.org/10.1002/2014GL061836

Moon, T., Joughin, I., Smith, B., & Howat, I. (2012). 21st-century evolution of Greenland outlet glacier velocities. *Science*, *336*(6081), 576–578.

Morlighem, M., Bondzio, J., Seroussi, H., Rignot, E., Larour, E., Humbert, A., & Rebuffi, S. (2016). Modeling of store gletscher's calving dynamics, West Greenland, in response to ocean thermal forcing. *Geophysical Research Letters*, *43*, 2659–2666. https://doi.org/10.1002/2016GL067695

Motyka, R. J., Hunter, L., Echelmeyer, K. A., & Connor, C. (2003). Submarine melting at the terminus of a temperate tidewater glacier, LeConte Glacier, Alaska, U.S.A. *Annals of Glaciology*, *36*(1), 57–65.

Nick, F. M., van der Veen, C. J., Vieli, A., & Benn, D. I. (2010). A physically based calving model applied to marine outlet glaciers and implications for the glacier dynamics. *Journal of Glaciology*, *56*(199), 781–794.

Nye, J. F. (1955). Comments on Dr Loewe's letter and notes on crevasses. *Journal of Glaciology*, *2*(17), 512–514.

O'Leary, M., & Christoffersen, P. (2013). Calving on tidewater glaciers amplified by submarine frontal melting. *The Cryosphere*, *7*(1), 119–128.

Petrovic, J. J. (2003). Review mechanical properties of ice and snow. *Journal of Materials Science*, *38*(1), 1–6.

Rignot, E., Box, J., Burgess, E., & Hanna, E. (2008). Mass balance of the Greenland ice sheet from 1958 to 2007. *Geophysical Research Letters*, *35*, L20502. https://doi.org/10.1029/2008GL035417

Rignot, E., Fenty, I., Xu, Y., Cai, C., & Kemp, C. (2015). Undercutting of marine-terminating glaciers in West Greenland. *Geophysical Research Letters*, *42*, 5909–5917. https://doi.org/10.1002/2015GL064236

Rignot, E., & Kanagaratnam, P. (2006). Changes in the velocity structure of the Greenland ice sheet. *Science*, *311*(5763), 986–990.

Rignot, E., Koppes, M., & Velicogna, I. (2010). Rapid submarine melting of the calving faces of West Greenland glaciers. *Nature Geoscience*, *3*(3), 187–191.

Rignot, E., Xu, Y., Menemenlis, D., Mouginot, J., Scheuchl, B., Li, X., et al. (2016). Modeling of ocean-induced ice melt rates of five West Greenland glaciers over the past two decades. *Geophysical Research Letters*, *43*, 6374–6382. https://doi.org/10.1002/2016GL068784

Röhl, K. (2006). Thermo-erosional notch development at fresh-water-calving Tasman glacier, New Zealand. *Journal of Glaciology*, *52*(177), 203–213.

Schulson, E. M. (1999). The structure and mechanical behavior of ice. *Journal of the Minerals, Metals & Materials Society*, *51*(2), 21–27.

Sciascia, R., Straneo, F., Cenedese, C., & Heimbach, P. (2013). Seasonal variability of submarine melt rate and circulation in an East Greenland fjord. *Journal of Geophysical Research: Oceans*, *118*, 2492–2506. https://doi.org/10.1002/jgrc.20142

Slater, D. A., Nienow, P. W., Goldberg, D. N., Cowton, T. R., & Sole, A. J. (2017). A model for tidewater glacier undercutting by submarine melting. *Geophysical Research Letters*, *44*, 2360–2368. https://doi.org/10.1002/2016GL072374

Todd, J., & Christoffersen, P. (2014). Are seasonal calving dynamics forced by buttressing from ice mélange or undercutting by melting? Outcomes from full-stokes simulations of Store Gletscher, West Greenland. *The Cryosphere*, *8*(6), 2353–2365.

Todd, J., Christoffersen, P., Zwinger, T., Råback, P., Chauché, N., Benn, D., et al. (2018). A full-stokes 3-D calving model applied to a large Greenlandic glacier. *Journal of Geophysical Research: Earth Surface*, *123*, 410–432. https://doi.org/10.1002/2017JF004349

Truffer, M., & Motyka, R. J. (2016). Where glaciers meet water: Subaqueous melt and its relevance to glaciers in various settings. *Reviews of Geophysics*, *54*, 220–239. https://doi.org/10.1002/2015RG000494

van den Broeke, M., Bamber, J., Ettema, J., Rignot, E., Schrama, E., van de Berg, W. J., et al. (2009). Partitioning recent Greenland mass loss. *Science*, *326*(5955), 984–986.

van der Veen, C. J. (2002). Calving glaciers. *Progress in Physical Geography*, *26*(1), 96–122.

van der Veen, C. J. (2013). *Fundamentals of glacier dynamics*. Boca Raton, FL: CRC Press.

Xu, Y., Rignot, E., Fenty, I., Menemenlis, D., & Flexas, M. (2013). Subaqueous melting of Store Glacier, West Greenland from three-dimensional, high-resolution numerical modeling and ocean observations. *Geophysical Research Letters*, *40*, 4648–4653. https://doi.org/10.1002/grl.50825